Sensors & Diagnostics

PAPER

View Article Online
View Journal | View Issue

Cite this: *Sens. Diagn.*, 2024, **3**, 147

Acid-promoted fluorescent probe for monitoring endogenous methylglyoxal in tumors and gastritis†

Weijia Xu,‡ Senyao Liu,‡ Wenwen Cao and Hu Xiong *

Received 29th August 2023,
Accepted 11th November 2023

DOI: 10.1039/d3sd00228d

rsc.li/sensors

Methylglyoxal (MGO) is an important dicarbonyl metabolite that plays a crucial role in a range of physiological and pathological processes. It is critical to develop precise methods for detecting MGO levels *in vivo* to better understand its role in disease progression. Herein, we report an MGO-activatable fluorescent probe **Cy-DNH$_2$** based on hemicyanine, which could rapidly and selectively detect MGO with a low LOD of 95 nM in an acidic microenvironment. In the presence of MGO, acidic pH could trigger **Cy-DNH$_2$** to turn on intense fluorescence within 3 min. Moreover, **Cy-DNH$_2$** was able to target lysosomes, allowing for the detection of endogenous MGO in living cells as well as the identification of elevated MGO levels in tumors and mouse models of gastritis. This work may provide a valuable tool for monitoring MGO under acidic conditions and diagnosing MGO-related diseases.

Introduction

Methylglyoxal (MGO) is a reactive dicarbonyl metabolite produced in all live cells during various metabolic processes such as glycolysis, threonine catabolism, and the polyol pathway.[1–3] As a highly active molecule, MGO can react with proteins, DNA, and lipids to form advanced glycation end products, resulting in irreversible cell structural damage and dysfunction, which is closely associated with pathologies of diverse human diseases including obesity, Alzheimer's disease, cardiovascular disease, and diabetes.[4–10] The detoxification method of MGO mainly relies on glyoxalase 1 and glyoxalase 2, which can convert MGO into non-toxic D-lactic acid to regulate the levels of MGO in cells.[11–14] Indeed, elevated levels of MGO have been observed in cancer cells due to the aerobic glycolysis pathway and are involved in tumor progression.[15] Gastritis is another common inflammatory metabolic disease with stomach mucosal injury, and it raises the risk of cancer.[16,17] So far, the main clinical diagnostic tool for gastritis is the combination of an X-ray barium meal and endoscope.[18,19] However, these methods are complicated to operate, so it is of great significance to develop simple and non-invasive ways for diagnosing gastritis. Compared with normal stomach, the upregulation of MGO concentration occurs in the development of gastritis, which can kill gastrointestinal bacteria such as *Helicobacter pylori*.[20] Therefore, accurate detection of MGO levels *in vivo* provides a new way for the diagnosis of tumors and gastritis, further elucidating its role in the progression of these diseases.

Although MGO plays an important role in physiological processes, the mechanism of its impact on complex living systems is poorly understood due to the lack of simple and effective detection methods. To date, high-performance liquid chromatography (HPLC) and liquid chromatography-mass spectrometry (LC-MS) analysis have been commonly employed for the detection of MGO in biological samples.[21,22] However, these methods suffer from complicated processing steps such as cell lysis and deproteinization, leading to low sensitivity and poor accuracy, and are not suitable for biological systems. In recent years, fluorescence imaging has attracted wide attention because of its advantages of high sensitivity, non-invasive visualization, and fast response speed.[23–28] At present, only a small number of "turn-on" fluorescent probes have been created for imaging MGO in cells and mice.[3,4,11,29–34] Nevertheless, most of these fluorescent probes require a long reaction time with MGO (usually 1–2 h), which is not suitable for real-time detection of variations in MGO levels *in vitro* and *in vivo*. Moreover, fluorescent probes exhibiting high organelle-targeting capability have been rarely reported. As an essential digestive organelle, lysosomes have an acidic environment and contain different kinds of enzymes for cellular metabolism, and dysfunction of lysosomes has been related to a wide variety of diseases such as cancer and gastroenteritis.[35] Thus, real-time monitoring and imaging of MGO levels in lysosomes

Research Center for Analytical Sciences, Tianjin Key Laboratory of Biosensing and Molecular Recognition, College of Chemistry, Nankai University, Tianjin 300071, China. E-mail: xionghu@nankai.edu.cn

† Electronic supplementary information (ESI) available. See DOI: https://doi.org/10.1039/d3sd00228d

‡ These authors contributed equally to this work.

will help the diagnosis of cancer and gastritis, while such a fluorescent probe that can rapidly detect MGO under acidic conditions is still elusive.

To address these challenges, we herein designed and synthesized a novel lysosome-targeting fluorescent probe, named **Cy-DNH$_2$**, for real-time monitoring MGO levels in tumors and gastritis. Probe **Cy-DNH$_2$** was synthesized *via* the Knoevenagel condensation reaction of electron-deficient benzo[*cd*]indolium and *o*-phenylenediamine that is an MGO-specific recognition unit. Under acidic conditions, it was able to rapidly recognize MGO and form an emissive product within 3 min, showing strong fluorescence at 545–580 nm. Moreover, **Cy-DNH$_2$** could sensitively and selectively detect exogenous and endogenous MGO in HeLa cells with a low limit of detection (LOD) value of 95 nM. Notably, it allowed the successful visualization of endogenous MGO fluctuations in mouse tumors and stomach of acute gastritis. To the best of our knowledge, **Cy-DNH$_2$** is the first acid-promoted fluorescent probe capable of specifically imaging MGO in lysosomes.

Experimental methods

Synthesis of fluorescent probe Cy-DNH$_2$

Synthesis of compound 6. Compound **2** (64.6 mg, 0.2 mmol) and compound **5** (67.3 mg, 0.2 mmol) were refluxed in a mixture of dry ethanol (15 mL) under a nitrogen atmosphere. The reaction mixture was stirred at 80 °C for 4 h. After the reaction was completed, the solvent was removed under reduced pressure, and the crude product was purified by flash column chromatography over silica gel using petroleum methanol/dichloromethane, affording products as purple solids (yield, 50.7%), ^{1}H NMR (400 MHz, CD_3OD): δ 9.16 (d, J = 7.6 Hz, 1H), 8.76 (d, J = 16.0 Hz, 1H), 8.65 (d, J = 8.0 Hz, 1H), 8.32 (d, J = 8.4 Hz, 1H), 8.27 (d, J = 7.2 Hz, 1H), 8.18–8.14 (m, 2H), 8.00–7.93 (m, 3H), 7.86 (d, J = 16.0 Hz, 1H), 4.90 (m, 2H), 1.66 (t, J = 7.2 Hz, 3H), 1.57 (s, 18H).

Synthesis of Cy-DNH$_2$. Compound **6** (64 mg, 0.1 mmol) was dissolved in 5 mL dry dichloromethane and 5 mL trifluoroacetic acid mixed solution, and stirred for 12 h under a nitrogen atmosphere at room temperature. The reaction was monitored by TLC; after the reaction was completed, the mixture solution was adjusted to neutral pH with saturated sodium bicarbonate solution, and extracted with DCM. The crude product was purified by flash column chromatography over silica gel using petroleum methanol/dichloromethane, affording products as blue-black solids (yield, 68.0%), ^{1}H NMR (400 MHz, CD_3OD): δ 8.88 (d, J = 7.6 Hz, 1H), 8.63 (d, J = 15.2 Hz, 1H), 8.38 (d, J = 8.0 Hz, 1H), 8.03–7.99 (m, 2H), 7.79 (m, 2H), 7.50 (d, J = 8.4 Hz, 1H), 7.43–7.35 (m, 2H), 6.79 (d, J = 8.0 Hz, 1H), 4.60 (q, J = 7.6 Hz, 2H), 1.57 (t, J = 7.2 Hz, 3H), ^{13}C NMR (100 MHz, CD_3OD): δ 163.50, 163.16, 155.02, 149.38, 141.07, 134.72, 132.12, 131.38, 131.18, 130.65, 130.20, 127.69, 127.06, 125.83, 119.50, 116.60, 115.67, 114.29, 107.36, 40.94, 14.85.

Fluorescence imaging in living cells

For exogenous MGO detection, HeLa cells were treated with **Cy-DNH$_2$** (5 μM) for 2 h and fixed with 4% paraformaldehyde for 5 min, then phosphate buffer solutions (pH 4.2) containing different concentrations of MGO (0, 5, 10, 20, 30 μM) were added. After incubation for 30 min, laser confocal imaging was performed.

For endogenous MGO detection, HeLa cells in DMEM medium were pretreated with curcumin (0, 5, 10, 20, 30 μM) for 6 h, then incubated with **Cy-DNH$_2$** (5 μM) for 2 h, and washed twice with PBS, then fresh medium was added for laser confocal imaging.

Fluorescence imaging *in vivo*

Female BALB/c mice (6–8 weeks old, 18–20 g) were purchased from Beijing Vital River Laboratory Animal Technology Co., Ltd. All animal experiments were approved by the Ethics Committee of Nankai University and carried out in accordance with the guidelines for animal experiments. The gastritis mouse model was established by intragastric administration of 200 μL anhydrous ethanol; 30 min later, **Cy-DNH$_2$** (1 mM, 150 μL) was administered intragastrically into the mice. The abdominal hair of the mouse was removed and imaged using an IVIS Lumina imaging system. Finally, the mice were euthanized, and their livers, lungs, hearts, kidneys, spleens, and intestines were immediately collected for *ex vivo* fluorescence imaging.

In order to generate a tumor-bearing mouse model, 4T1-luc cells (2×10^5) were injected subcutaneously into the left and right hind limbs. After one week, the right leg tumor (experimental group) was injected with curcumin (200 μM, 50 μL) and pretreated for 6 h, while the left leg tumor (control group) was injected with the same amount of PBS. Then, **Cy-DNH$_2$** (500 μM, 50 μL) was injected into the left and right tumors, respectively. 2 hours later, fluorescence imaging was performed using an IVIS imaging system (λ_{ex} = 556 nm, λ_{em} = 580–640 nm).

Results and discussion

Design and synthesis of MGO-activatable probe Cy-DNH$_2$

Hemicyanine dyes have been broadly used in the fields of biological imaging and disease diagnosis due to their high stability, large Stokes shift, tunable spectral characteristics, and good biocompatibility.[36] Here, MGO-activatable probe **Cy-DNH$_2$** with a hemicyanine structure was constructed by the Knoevenagel condensation reaction (Scheme 1). *O*-Phenylenediamine, an MGO-specific recognition unit, was

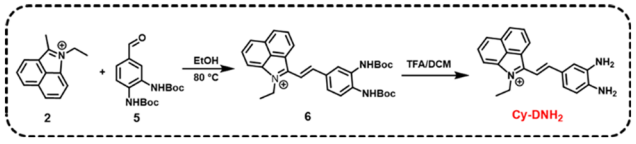

Scheme 1 Synthetic route of **Cy-DNH$_2$**.

selected to detect MGO with excellent selectivity.[30] Under acidic conditions, **Cy-DNH$_2$** could rapidly react with MGO to form the structure of quinoxaline (Fig. 1a). Once reacted with MGO, the donor–π–acceptor (D–π–A) skeleton of **Cy-DNH$_2$** was changed, showing intense "turn-on" fluorescence emission. As shown in Fig. 1b and c, the maximum absorption wavelength of **Cy-DNH$_2$** was 590 nm. After reacting with MGO, the absorption wavelength of the probe blue-shifted, and a new absorption peak appeared at 460 nm due to the change in donor–acceptor electron properties. The fluorescence intensity of **Cy-DNH$_2$** was very weak, and the fluorescence signal at 545 nm was greatly enhanced after the reaction with MGO. Then, Fourier transform high-resolution mass spectrometry (FTMS) was used to analyze the charge-mass ratio (m/z) of **Cy-DNH$_2$** and the product of **Cy-DNH$_2$** with MGO. Compared with the characteristic peak of **Cy-DNH$_2$** (m/z = 314.1654), the product showed a strong response peak at m/z of 350.1654, indicating that the reaction between **Cy-DNH$_2$** and MGO formed a quinoxaline structure with the loss of two water molecules (Fig. 1d and e). To further understand the fluorescence response mechanism, density functional theory (DFT) calculation was used to optimize the structure and electron distribution of **Cy-DNH$_2$** in the excited state treated with or without MGO. As shown in Fig. S1,† both of them exhibited similar highest occupied molecular orbital (HOMO) and lowest unoccupied molecular orbital (LUMO) distributions. However, it was found that the dihedral angle between the donor and the acceptor of **Cy-DNH$_2$** is 89°, almost in a vertical conformation, whose charge transfer state is typically not favored for radiative fluorescence emission.[37] By contrast, after MGO treatment, the dihedral angle between the donor and the acceptor plane decreases to 27°, which could facilitate intermolecular charge transfer and enhance radiative transition with bright fluorescence.

Spectroscopic properties of Cy-DNH$_2$ towards MGO

Then, in order to further study the response of **Cy-DNH$_2$** towards different concentrations of MGO, we measured the fluorescence spectra of 10 μM **Cy-DNH$_2$** reacted with different concentrations of MGO. The results are shown in Fig. 2a; as the MGO content increases (0–150 μM), the fluorescence signals at 545–570 nm gradually increased. In addition, the fluorescence intensity at 545 nm also showed a good linear relationship with the concentration of MGO in the range of 0–30 μM (R^2 = 0.998), and the limit of detection (LOD, 3σ/slope) was 95 nM (Fig. 2b), indicating that this probe could detect MGO sensitively and quantitatively. Next, we further investigate the pH effects on the reactivity of the MGO probe. **Cy-DNH$_2$** (10 μM) and MGO (100 μM) were co-incubated in different pH buffers at 37 °C for 30 min, and then their fluorescence emission spectra were measured. As shown in Fig. 2c, under the condition of low pH (3–5), **Cy-DNH$_2$** exhibited higher fluorescence response intensity towards MGO, indicating that this pH-dependent fluorescence enhancement phenomenon was probably attributed to the process of condensation reaction. To further investigate this effect, we next examined the reaction between **Cy-DNH$_2$** and MGO with or without acid. When **Cy-DNH$_2$** was treated with

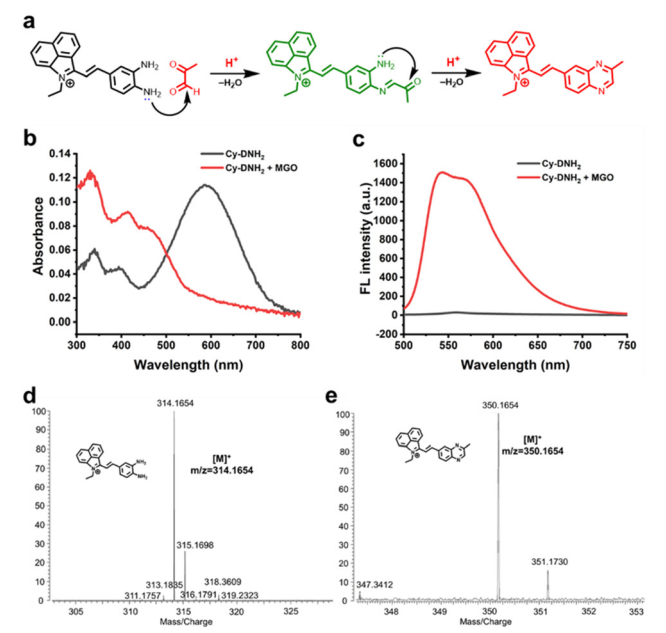

Fig. 1 (a) Proposed reaction mechanism of **Cy-DNH$_2$** towards MGO under acidic conditions. Absorption spectra (b) and fluorescence emission spectra (c) of 10 μM **Cy-DNH$_2$** and **Cy-DNH$_2$** incubated with 100 μM MGO in pH 4.2 buffer. λ_{ex} = 470 nm. Mass spectra of **Cy-DNH$_2$** (d) and **Cy-DNH$_2$** reacted with MGO (e).

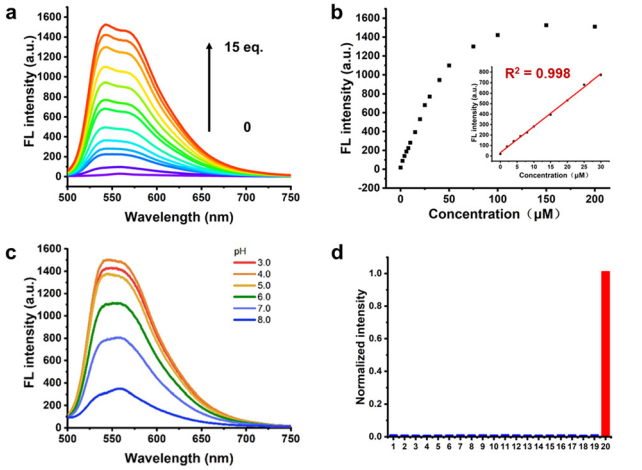

Fig. 2 (a) Fluorescence response spectra of 10 μM **Cy-DNH$_2$** in the presence of different concentrations of MGO, λ_{ex} = 470 nm. (b) Plot of fluorescence intensity of **Cy-DNH$_2$** at 545 nm as a function of MGO concentration. Inset: The linear relationship between fluorescence intensity and MGO concentration in the range of 0–30 μM. (c) Fluorescence response spectra of **Cy-DNH$_2$** to MGO in different pH buffers. (d) Relative fluorescence intensity at 545 nm of 10 μM **Cy-DNH$_2$** treated with various species (200 μM) in pH 4.2 buffers (1. blank, 2. L-Arg, 3. L-Cys, 4. L-Lys, 5. L-Try, 6. GSH, 7. Ca^{2+}, 8. Cu^{2+}, 9. Fe^{2+}, 10. NH_4^+, 11. SO_3^{2-}, 12. ClO^-, 13. $H_2PO_4^-$, 14. NO_2^-, 15. NO_3^-, 16. NO, 17. ·OH, 18. $O_2^{\cdot-}$, 19. H_2O_2, 20. MGO).

only MGO or trifluoroacetic acid (TFA), there was no fluorescence increase within 5 min. However, the fluorescence intensity increased rapidly in the presence of both MGO and TFA, reaching a plateau within 3 min (Fig. S2†). These results confirmed that acidic pH could significantly accelerate the reaction of the probe with MGO. To further evaluate its selectivity towards MGO, we measured the fluorescence spectra of **Cy-DNH$_2$** (10 μM) incubated with a variety of common biological species (Fig. 2d and S3†). Among all species (except glyoxal), only MGO could remarkably turn on the fluorescence of **Cy-DNH$_2$**, while no obvious changes were observed in the presence of other species. It is worth noting that *o*-phenylenediamine has also been reported to respond with nitric oxide (NO),[23] but this probe did not turn on in the presence of 20 equiv. NO. Then, we increased the concentration of NO over hundreds of equivalents, and we found that **Cy-DNH$_2$** could slightly turn on its fluorescence. Because the concentration of NO in cells is much lower than that, therefore, **Cy-DNH$_2$** can selectively detect MGO without interference of NO and holds great promise for applications in living systems.

Cellular localization and fluorescence imaging of MGO in cells

Before cell imaging, we first evaluated the cytotoxicity of **Cy-DNH$_2$** by CCK-8 assay. As shown in Fig. S4,† HeLa cells retained a high survival rate with **Cy-DNH$_2$** at the concentrations from 0 to 25 μM, indicating its high biocompatibility. Later, we examined the organelle-targeting ability of **Cy-DNH$_2$**; HeLa cells were incubated with **Cy-DNH$_2$** and commercial mitochondria or lysosome targeting probes. The results are shown in Fig. 3a and S5;† the red channels were the fluorescence signals from **Cy-DNH$_2$**, while the green channels were the fluorescence signals from mitochondria or lysosome trackers. **Cy-DNH$_2$** was co-localized well with lysosomes and not with mitochondria, showing a Pearson coefficient of 0.86 and 0.68, respectively. Since it has a better response to MGO under acidic pH conditions, **Cy-DNH$_2$** is promising for monitoring MGO levels in lysosomes.

Next, we investigated the ability of **Cy-DNH$_2$** for cellular MGO imaging in the lysosomes of living cells by confocal microscopy. The HeLa cells were pre-incubated with **Cy-DNH$_2$** for 2 h and treated with MGO for 30 min. As shown in Fig. S6,† the fluorescence intensity of cells treated with exogenous MGO was not significantly enhanced compared with untreated cells, which was probably ascribed to the fast MGO consumption by glyoxalase 1 (GLO1) in cells.[11] In order to eliminate the interference of cellular metabolism of MGO, HeLa cells were fixed with paraformaldehyde before imaging. After being incubated with **Cy-DNH$_2$**, HeLa cells were fixed and treated with different concentrations of MGO (0–30 μM) for 30 min in pH 4.2 phosphate buffers. As shown in Fig. 3b and c, with the increase of exogenous MGO, significant red fluorescence signals emerged and enhanced gradually, demonstrating the high ability of **Cy-DNH$_2$** to detect MGO in cells. To further assess the pH effect on MGO detection in cells, we incubated HeLa cells with **Cy-DNH$_2$** in buffers (containing 10 μM MGO) of pH 4.2 and 7.4, respectively. HeLa cells treated with acidic buffer displayed higher fluorescence intensity (Fig. S7†), suggesting that the lysosome-targeting ability of **Cy-DNH$_2$** contributes to MGO detection in cells due to the acidic microenvironment of lysosomes.

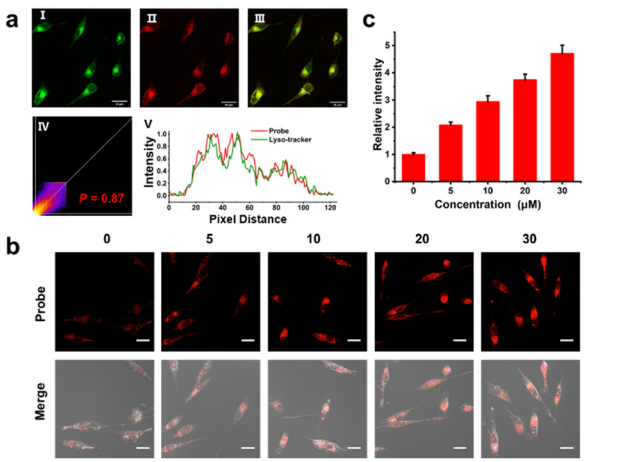

Fig. 3 (a) Colocalization imaging of HeLa cells stained with **Cy-DNH$_2$** (10 μM) and Lyso-Tracker Green (1 μM). (I) Green channel (Lyso-Tracker Green, λ_{ex} = 487 nm, λ_{em} = 500–550 nm). (II) Red channel (**Cy-DNH$_2$**, λ_{ex} = 487 nm, λ_{em} = 570–620 nm). (III) Merged image of (I and II). (IV) Intensity scatter plot. (V) Relative intensity profile of the white line across HeLa cells. Scale bar = 25 μm. (b) Confocal fluorescence images of **Cy-DNH$_2$** stained HeLa cells in response to different concentrations of MGO (λ_{ex} = 487 nm, λ_{em} = 570–620 nm), scale bar: 20 μm. (c) Relative fluorescence intensity of cells in (b).

Monitoring endogenous MGO elevation in cells and mice

Furthermore, we applied **Cy-DNH$_2$** to monitor the endogenous MGO levels in living cells. Typically, cancer cells can overexpress the GLO1 enzyme to detoxify the excessive MGO generated in the glycolytic pathway, and thus inhibition of the GLO1 activity will increase the MGO levels in cancer cells.[11] Curcumin, as one of the inhibitors of GLO1, can effectively increase the accumulation of MGO in cells. As shown in Fig. 4a and b, untreated HeLa cells showed low red fluorescence. In contrast, after being treated with curcumin for 6 h, HeLa cells exhibited strong red fluorescence due to the accumulation of excessive MGO, and the fluorescence intensity increased with the increase in curcumin concentration. These results revealed that **Cy-DNH$_2$** might be used not only to detect MGO in cells, but also to monitor the ability of GLO1 inhibitors to promote MGO accumulation in cells, and even utilized to screen GLO1 inhibitors at the cellular level in the future.

Encouraged by the cell imaging results, we next evaluated the feasibility of **Cy-DNH$_2$** to detect MGO in tumors. The tumor-bearing mouse model was established by injecting 4T1 cells into the right and left legs of the mouse (Fig. 4c). After

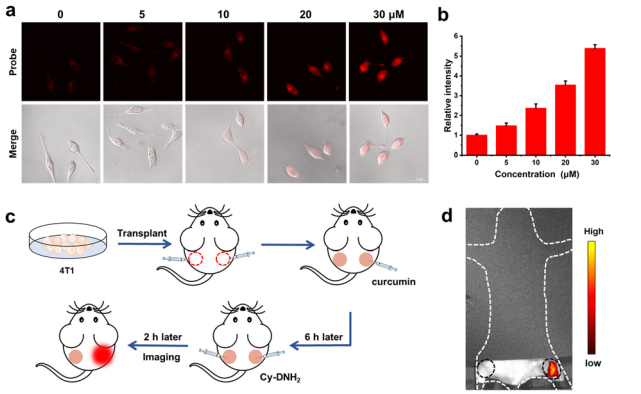

Fig. 4 (a) Confocal fluorescence imaging of curcumin-induced endogenous MGO in HeLa cells stained with **Cy-DNH$_2$** (λ_{ex} = 487 nm, λ_{em} = 570–620 nm), scale bar: 20 μm. (b) Relative fluorescence intensity of cells in (a). (c) The establishment of the tumor model for endogenous MGO detection *in vivo*. (d) Fluorescence imaging of tumors in left and right legs.

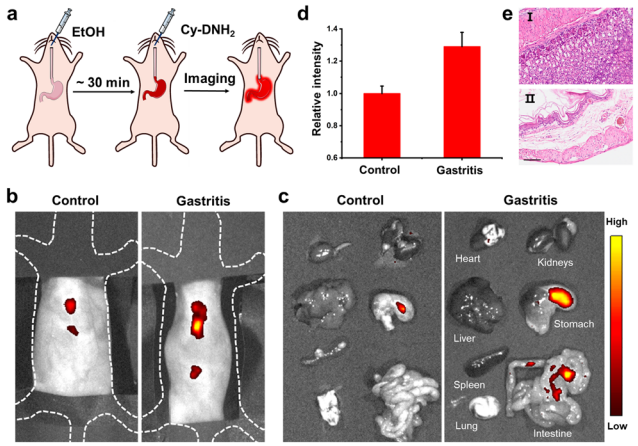

Fig. 5 (a) Construction of a mouse model of acute gastritis. (b) Fluorescence images of the control mouse and gastritis mouse. (c) Representative *ex vivo* fluorescence images of major organs. (d) Relative fluorescence intensity around the stomach in (b). (e) H&E staining analysis of stomach tissues in the normal mouse (I) and the gastritis mouse (II), scale bar = 100 μm.

one week, PBS (~50 μL) and curcumin (~50 μL, 100 μM) were injected into the left and right tumors, respectively. 6 hours later, **Cy-DNH$_2$** was injected into the tumors of the left and right legs. After 2 hours, fluorescence imaging was performed. As shown in Fig. 4d, there was much stronger fluorescence intensity in the right tumor than that in the control left tumor, which was consistent with the results of cell imaging. Therefore, these results demonstrated that **Cy-DNH$_2$** has good capability to image endogenous MGO and elevated levels of MGO appearing in tumors induced by GLO1 inhibitor curcumin.

Fluorescence imaging of MGO in the gastritis mouse model

Gastritis is one of the most common inflammatory metabolic diseases; if not treated in time, it might develop into gastric cancer. There remains a need to develop non-invasive methods for diagnosis of gastritis. Previous studies have shown that an increase in MGO levels was observed in inflammatory gastrointestinal cells.[17] To demonstrate the potential of **Cy-DNH$_2$** to visualize MGO in a stomach with gastritis, a mouse model of gastritis was established by intragastric administration of alcohol (Fig. 5a).[38] 30 min later, 150 μL of **Cy-DNH$_2$** was injected into the stomachs of the mice, and fluorescence imaging was performed. The fluorescence signals of mice with gastritis were significantly higher than those of healthy mice (Fig. 5b and d). Then, we collected the major organs of the mice, including the stomach, and found that the stomach with gastritis showed stronger fluorescence intensity (Fig. 5c). In addition, compared with the normal stomach, obvious swelling, superficial mucosal congestion, and fibrous tissue hyperplasia were observed in the stomach with gastritis. The results of H&E staining further verified the successful establishment of gastritis (Fig. 5e). Therefore, **Cy-DNH$_2$** has great potential as a useful fluorescent tool in the diagnosis of gastritis.

Conclusions

Here, we developed an acid-promoted fluorescent probe **Cy-DNH$_2$** for monitoring MGO levels in tumors and gastritis. Compared with previously reported probes, **Cy-DNH$_2$** has high sensitivity and good selectivity to MGO in an acidic environment, showing a low LOD of 95 nM. It can not only image the accumulation of endogenous MGO in lysosomes of cells, but also monitor the GLO1 activity in the tumor-bearing mouse model. Furthermore, **Cy-DNH$_2$** was successfully applied to visualize the up-regulation of MGO levels in the gastritis mouse model. Taken together, **Cy-DNH$_2$** is a promising fluorescent probe for the detection of MGO under acidic conditions.

Author contributions

W. X. and H. X. designed the research; W. X., S. L. and W. C. performed the experiments. W. X., S. L. and H. X. analyzed the data; W. X. and H. X. wrote the paper; H. X. supervised the research.

Conflicts of interest

The authors declare no competing financial interest.

Acknowledgements

This work was supported by the National Natural Science Foundation of China (22174078) and the Fundamental Research Funds for the Central Universities, Nankai University (63221408).

Notes and references

1 H. Wang, Y. Xu, L. Rao, C. Yang, H. Yuan, T. Gao, X. Chen, H. Sun, M. Xian, C. Liu and C. Liu, *Anal. Chem.*, 2019, **91**, 5646–5653.
2 Y. Guo, Y. Zhang, X. Yang, P. Lu, X. Yan, F. Xiao, H. Zhou, C. Wen, M. Shi, J. Lu and Q. H. Meng, *Cancer Biol. Ther.*, 2016, **17**, 169–180.
3 Y. Lai, Y. Dang, Q. Sun, J. Pan, H. Yu, W. Zhang and Z. Xu, *Chem. Sci.*, 2022, **13**, 12511–12518.
4 M. Yang, J. Fan, J. Zhang, J. Du and X. Peng, *Chem. Sci.*, 2018, **9**, 6758–6764.
5 S. S. More, A. P. Vartak and R. Vince, *ACS Chem. Neurosci.*, 2013, **4**, 330–338.
6 Q. Xie, Y. Zhan, L. Guo, H. Hao, X. Shi, J. Yang, F. Luo, B. Qiu and Z. Lin, *ChemistryOpen*, 2022, **11**, e202200055.
7 D. Prantner, S. Nallar, K. Richard, D. Spiegel, K. D. Collins and S. N. Vogel, *J. Leukocyte Biol.*, 2021, **109**, 605–619.
8 S. Koike, C. Ando, Y. Usui, Y. Kibune, S. Nishimoto, T. Suzuki and Y. Ogasawara, *Brain Res. Bull.*, 2019, **144**, 164–170.
9 C. Sibbersen, J. Palmfeldt, J. Hansen, N. Gregersen, K. A. Jorgensen and M. Johannsen, *Chem. Commun.*, 2013, **49**, 4012–4014.
10 D. J. Selkoe, *Science*, 2002, **298**, 789–791.
11 C. Ding, F. Wang, Y. Dang, Z. Xu, L. Li, Y. Lai, H. Yu, Y. Luo, R. Huang, A. Zhang and W. Zhang, *Anal. Chem.*, 2019, **91**, 15577–15584.
12 K. O. Alfarouk, S. S. Alqahtani, S. Alshahrani, J. Morgenstern, C. T. Supuran and S. J. Reshkin, *J. Enzyme Inhib. Med. Chem.*, 2021, **36**, 2010–2015.
13 M. Cnop, F. Foufelle and L. A. Velloso, *Trends Mol. Med.*, 2012, **18**, 59–68.
14 Y. Dang, Y. Lai, F. Chen, Q. Sun, C. Ding, W. Zhang and Z. Xu, *Anal. Chem.*, 2022, **94**, 1076–1084.
15 A. Bellahcene, M. J. Nokin, V. Castronovo and C. Schalkwijk, *Semin. Cancer Biol.*, 2018, **49**, 64–74.
16 C. J. Chao, J. S. Shin, W. C. Hsu and P. M. Wang, *Endoscopy*, 2013, **45**, E280–E281.
17 K. Sugano, J. Tack, E. J. Kuipers, D. Y. Graham, E. M. El-Omar, S. Miura, K. Haruma, M. Asaka, N. Uemura and P. Malfertheiner, *Gut*, 2020, **70**, 431–432.
18 I. L. P. Beales, *Gut*, 2020, **70**, 431–432.
19 Y. Wu, J. Gu, S. Zhang, Y. Gu, J. Ma, Y. Wang, L. W. Zhang and Y. Wang, *Anal. Chem.*, 2021, **93**, 6414–6420.
20 S. Brighina, C. P. Turrado, C. Restuccia, G. Walton, B. Fallico, M. J. Oruna-Concha and E. Arena, *Food Chem.*, 2021, **341**, 128237.
21 G. Liu, Q. Xia, Y. Lu, T. Zheng, S. Sang and L. Lv, *J. Agric. Food Chem.*, 2017, **65**, 2233–2239.
22 M. Y. Wu, B. G. Chen, C. D. Chang, M. H. Huang, T. G. Wu, D. M. Chang, Y. J. Lee, H. C. Wang, C. I. Lee, C. L. Chern and R. H. Liu, *J. Chromatogr. A*, 2008, **1204**, 81–86.
23 S. Liu, Y. Zhu, P. Wu and H. Xiong, *Anal. Chem.*, 2021, **93**, 4975–4983.
24 P. Wu, Y. Zhu, S. Liu and H. Xiong, *ACS Cent. Sci.*, 2021, **7**, 2039–2048.
25 W. Xu, S. Liu, Z. Chen, F. Wu, W. Cao, Y. Tian and H. Xiong, *Anal. Chem.*, 2022, **94**, 13556–13565.
26 S. Liu, W. Xu, X. Li, D.-W. Pang and H. Xiong, *ACS Nano*, 2022, **16**, 17424–17434.
27 W.-X. Wang, W.-L. Jiang, G.-J. Mao, M. Tan, J. Fei, Y. Li and C.-Y. Li, *Anal. Chem.*, 2021, **93**, 3301–3307.
28 L. Yan, Q.-S. Gu, W.-L. Jiang, M. Tan, Z.-K. Tan, G.-J. Mao, F. Xu and C.-Y. Li, *Anal. Chem.*, 2022, **94**, 5514–5520.
29 S. T. Wang, Y. Lin, C. D. Spicer and M. M. Stevens, *Chem. Commun.*, 2015, **51**, 11026–11029.
30 T. Wang, E. F. Douglass, K. J. Fitzgerald and D. A. Spiege, *J. Am. Chem. Soc.*, 2013, **135**, 12429–12433.
31 H. Xu, Q. Liu, X. Song, C. Wang, X. Wang, S. Ma, X. Wang, Y. Feng, X. Meng, X. Liu, W. Wang and K. Lou, *Anal. Chem.*, 2020, **92**, 13829–13838.
32 W. Zhang, F. Zhang, Y. L. Wang, B. Song, R. Zhang and J. Yuan, *Inorg. Chem.*, 2017, **56**, 1309–1318.
33 Y. Dang, F. Wang, L. Li, Y. Lai, Z. Xu, Z. Xiong, A. Zhang, Y. Tian, C. Ding and W. Zhang, *Chem. Commun.*, 2020, **56**, 707–710.
34 Z. Wang, Y. Bian, C. Liu, S. He, L. Zhao and X. Zeng, *Chem. Commun.*, 2022, **58**, 6453–6456.
35 A. Ballabio and J. S. Bonifacino, *Nat. Rev. Mol. Cell Biol.*, 2020, **21**, 101–118.
36 Z. Zeng, S. S. Liew, X. Wei and K. Pu, *Angew. Chem., Int. Ed.*, 2021, **60**, 26454–26475.
37 M. Lv, Y. Yu, M. E. Sandoval-Salinas, J. Xu, Z. Lei, D. Casanova, Y. Yang and J. Chen, *Angew. Chem., Int. Ed.*, 2020, **59**, 22179–22184.
38 Y. Tian, Z. Chen, S. Liu, F. Wu, W. Cao, D.-W. Pang and H. Xiong, *Angew. Chem., Int. Ed.*, 2023, **62**, e202309768.